

[REDACTED]
[REDACTED]
[REDACTED]
[REDACTED]

[REDACTED]
[REDACTED]
[REDACTED]

In [2], [3], [4], [5], [6], [7], [8], [9], [10], [11], [12], [13], [14], [15], [16], [17], [18], [19], [20], [21], [22], [23], [24], [25], [26], [27], [28], [29], [30], [31], [32], [33], [34], [35], [36], [37], [38], [39], [40], [41], [42], [43], [44], [45], [46], [47], [48], [49], [50], [51], [52], [53], [54], [55], [56], [57], [58], [59], [60], [61], [62], [63], [64], [65], [66], [67], [68], [69], [70], [71], [72], [73], [74], [75], [76], [77], [78], [79], [80], [81], [82], [83], [84], [85], [86], [87], [88], [89], [90], [91], [92], [93], [94], [95], [96], [97], [98], [99], [100].

$$\begin{aligned}
 r_1(x_1, x_2) &= \frac{-x_1}{2\pi(x_1^2 + x_2^2)^{3/2}} \\
 r_2(x_1, x_2) &= \frac{-x_2}{2\pi(x_1^2 + x_2^2)^{3/2}}
 \end{aligned} \tag{1}$$

where $f_M = (f, f_R) = (f, r_1 * f, r_2 * f)$, $f_R = (f, r_1(x_1, x_2), r_2(x_1, x_2))$, and $R = (r_1, r_2)$. In [54], In [55], In [56], In [57], In [58], In [59], In [60], In [61], In [62], In [63], In [64], In [65], In [66], In [67], In [68], In [69], In [70], In [71], In [72], In [73], In [74], In [75], In [76], In [77], In [78], In [79], In [80], In [81], In [82], In [83], In [84], In [85], In [86], In [87], In [88], In [89], In [90], In [91], In [92], In [93], In [94], In [95], In [96], In [97], In [98], In [99], In [100].

$$C(w) = n_c |w|^a \quad (-s |w|), a \geq 1 \tag{2}$$

where $w = (w_1, w_2)$, $n_c = \left(\frac{\pi 4^{a+1} s^{2a+1}}{\Gamma(2a+1)}\right)^{\frac{1}{2}}$, $\Gamma(\cdot)$ is the Gamma function, $a = 1.58$, $W = 1$, [39]. In [44], In [45], In [46], In [47], In [48], In [49], In [50], In [51], In [52], In [53], In [54], In [55], In [56], In [57], In [58], In [59], In [60], In [61], In [62], In [63], In [64], In [65], In [66], In [67], In [68], In [69], In [70], In [71], In [72], In [73], In [74], In [75], In [76], In [77], In [78], In [79], In [80], In [81], In [82], In [83], In [84], In [85], In [86], In [87], In [88], In [89], In [90], In [91], In [92], In [93], In [94], In [95], In [96], In [97], In [98], In [99], In [100].

$$PA = \sum_s \frac{[|o_s| - |e_s| - T_s]}{\sqrt{e_s^2 + o_s^2 + \varepsilon}} \tag{3}$$

where PA is the performance index, ε is a small positive constant, T_s is the threshold, o_s and e_s are the observed and expected values, respectively, and C_k is the k -th order central moment. In [54], In [55], In [56], In [57], In [58], In [59], In [60], In [61], In [62], In [63], In [64], In [65], In [66], In [67], In [68], In [69], In [70], In [71], In [72], In [73], In [74], In [75], In [76], In [77], In [78], In [79], In [80], In [81], In [82], In [83], In [84], In [85], In [86], In [87], In [88], In [89], In [90], In [91], In [92], In [93], In [94], In [95], In [96], In [97], In [98], In [99], In [100].

Figure 1 shows the performance index PA versus the threshold T_s for different values of s : $s = 5$, $s = 10$, $s = 20$, $s = 25$, and $s = 15$. The performance index PA increases as the threshold T_s increases and as the value of s increases. In [54], In [55], In [56], In [57], In [58], In [59], In [60], In [61], In [62], In [63], In [64], In [65], In [66], In [67], In [68], In [69], In [70], In [71], In [72], In [73], In [74], In [75], In [76], In [77], In [78], In [79], In [80], In [81], In [82], In [83], In [84], In [85], In [86], In [87], In [88], In [89], In [90], In [91], In [92], In [93], In [94], In [95], In [96], In [97], In [98], In [99], In [100].

Fig. 1. Performance index PA versus the threshold T_s for different values of s : (a) $T_s = 0$, (b) $T_s = 5$, (c) $T_s = 10$, (d) $T_s = 15$, (e) $T_s = 20$, (f) $T_s = 25$.

In [61], In [62], In [63], In [64], In [65], In [66], In [67], In [68], In [69], In [70], In [71], In [72], In [73], In [74], In [75], In [76], In [77], In [78], In [79], In [80], In [81], In [82], In [83], In [84], In [85], In [86], In [87], In [88], In [89], In [90], In [91], In [92], In [93], In [94], In [95], In [96], In [97], In [98], In [99], In [100].

B. Fractional-Order Differential

The fractional-order differential $D^\alpha f(x)$ is defined as [47], $f(x) \in L^2(R)$, where R is the real line.

$$D^\alpha f(x) = \frac{d^\alpha f(x)}{dx^\alpha} \tag{4}$$

where α is the fractional order, T is the time, and F is the Fourier transform.

$$\begin{aligned}
 D^\alpha f(x) &\stackrel{FT}{\Leftrightarrow} (\hat{D}^\alpha f)(w) = (iw)^\alpha \hat{f}(w) \\
 &= |w|^\alpha [i\theta^\alpha(w)] \hat{f}(w) \\
 &= |w|^\alpha \left[\frac{\alpha\pi i}{2}, n(w)\right] \hat{f}(w)
 \end{aligned} \tag{5}$$

where w is the angular frequency, $n(\cdot)$ is the phase, and $[i\theta^\alpha(w), n(w)]$ is the complex number. In [61], In [62], In [63], In [64], In [65], In [66], In [67], In [68], In [69], In [70], In [71], In [72], In [73], In [74], In [75], In [76], In [77], In [78], In [79], In [80], In [81], In [82], In [83], In [84], In [85], In [86], In [87], In [88], In [89], In [90], In [91], In [92], In [93], In [94], In [95], In [96], In [97], In [98], In [99], In [100].

2. The total variation of the image \$f(x)\$ is defined as follows:

The total variation of the image \$f(x)\$ is defined as follows:

The total variation of the image \$f(x)\$ is defined as follows:

The total variation of the image \$f(x)\$ is defined as follows:

The total variation of the image \$f(x)\$ is defined as follows:

The total variation of the image \$f(x)\$ is defined as follows:

The total variation of the image \$f(x)\$ is defined as follows:

The total variation of the image \$f(x)\$ is defined as follows:

The total variation of the image \$f(x)\$ is defined as follows:

$$D^\alpha f(x) \triangleq \lim_{h \rightarrow 0} \frac{1}{h^\alpha} \sum_{l=0}^{[\frac{d-c}{h}]} (-1)^l \binom{\alpha}{l} f(x - lh) \quad (6)$$

The total variation of the image \$f(x)\$ is defined as follows:

$$\binom{\alpha}{l} = \frac{\Gamma(\alpha + 1)}{\Gamma(l + 1)\Gamma(\alpha - l + 1)} \quad (7)$$

The total variation of the image \$f(x)\$ is defined as follows:

Fractional-Order AD Filter and Fractional-Order AD Filter

The total variation of the image \$f(x)\$ is defined as follows:

$$\frac{\partial u}{\partial t} = \text{div} [c(|\nabla u|) \cdot \nabla u], \quad (8)$$

The total variation of the image \$f(x)\$ is defined as follows:

... λ ... ;
 ... λ ...
 ... T ...
 ... In ...
 ... PSNR ...
 ... [60]. W ... 0.01 ...
 ... R ...
 ... PAS ...

$$\begin{cases} \varphi = (PA - 1)^2 \\ \gamma = PA(2 - PA) \end{cases} \quad (15)$$

... PA ...
 ... PA ... 0,
 ... FAD ...
 ... W n PA ... 1, ... FTV ...
 ... PA ... 1,
 ... FAD ...
 ... H ... FAD ...
 ... PAS ...
 ... PAS ...
 ... W ...
 ... f(| $\nabla^\alpha u$) ...
 ... (12). T ...

$$c(|\nabla^\alpha u|, PA) = 1 / \left[1 + \frac{|\nabla^\alpha u| \cdot (1 + 254 \cdot PA)}{k_1^2} \right] \quad (16)$$

... $k_1 = k_0 e^{-0.05(n_{iter}-1)}$... (9).
 ... n_{iter} ...
 ... A ...
 ... II-B, ...
 ... PAS ...
 ... S ...
 ... [46]

$$\alpha = 1 + \frac{1}{2} (1 + PA^2) \quad (17)$$

... PA ... PAS ... T ...
 ... $\alpha \in (1, 2)$. T ... PFDTV ...
 ... PAS ...
 ... In ... PAS ...
 ... A ... PAS ...

... n ... n ... n ...
 ... n ... A ... (17), ... PAS ...
 ... r ... α ...
 ... PFDTV ...
 ... n ...
 ... n ...
 ... n ...

B. Numerical Solver

W ... E ...-L ... [61]
 ... n ... (14). A ...
 ... n ... E(u) ...
 ... In ...
 ... u ...
 ... 0, ...
 ... 0. T ...
 ... $\eta \in C^\infty(\Omega)$...
 ... e. D :

$$\begin{aligned} \Phi(e) &:= E(u + e\eta) \\ &= \int_{\Omega} [\varphi f(|\nabla^\alpha(u + e\eta)|) + \gamma |\nabla^\alpha(u + e\eta)|] dx dy \\ &\quad + \int_{\Omega} \left(\frac{\lambda}{2} |u + e\eta - u_0|^2 \right) dx dy \end{aligned} \quad (18)$$

W ... $\Phi(e)$...

$$\begin{aligned} \Phi'(e) &= \frac{d}{de} \Phi(e) \\ &= \varphi \int_{\Omega} \left(f'(|\nabla^\alpha(u + e\eta)|) \right. \\ &\quad \times \left. \frac{\nabla_x^\alpha(u + e\eta) \nabla_x^\alpha \eta + \nabla_y^\alpha(u + e\eta) \nabla_y^\alpha \eta}{\sqrt{(\nabla_x^\alpha(u + e\eta))^2 + (\nabla_y^\alpha(u + e\eta))^2}} \right) dx dy \\ &\quad + \gamma \int_{\Omega} \left(\frac{\nabla_x^\alpha(u + e\eta) \nabla_x^\alpha \eta + \nabla_y^\alpha(u + e\eta) \nabla_y^\alpha \eta}{\sqrt{(\nabla_x^\alpha(u + e\eta))^2 + (\nabla_y^\alpha(u + e\eta))^2}} \right) dx dy \\ &\quad + \lambda \int_{\Omega} (u + e\eta - u_0) \eta dx dy, \end{aligned} \quad (19)$$

L ... $e = 0$, ...

$$\begin{aligned} \Phi'(0) &= \varphi \int_{\Omega} \left(c(|\nabla^\alpha u|^2, PA^2) \left(\nabla_x^\alpha u \nabla_x^\alpha \eta + \nabla_y^\alpha u \nabla_y^\alpha \eta \right) \right) dx dy \\ &\quad + \gamma \int_{\Omega} \frac{\nabla_x^\alpha u \nabla_x^\alpha \eta + \nabla_y^\alpha u \nabla_y^\alpha \eta}{|\nabla^\alpha u|} dx dy \\ &\quad + \lambda \int_{\Omega} (u - u_0) \eta dx dy \end{aligned} \quad (20)$$

$$|\nabla^\alpha u| = \sqrt{(\nabla_x^\alpha u)^2 + (\nabla_y^\alpha u)^2}$$

$$\Phi'(0) = 0, \quad (20)$$

$$\nabla_x^\alpha u \nabla_x^\alpha \eta + \nabla_y^\alpha u \nabla_y^\alpha \eta = \left((\nabla_x^\alpha)^* \nabla_x^\alpha u + (\nabla_y^\alpha)^* \nabla_y^\alpha u \right) \eta \quad (21)$$

[62]. By [62], we have

$$\begin{aligned} \Phi'(0) &= \varphi \int_{\Omega} c(|\nabla^\alpha u|^2, PA^2) \left((\nabla_x^\alpha)^* \nabla_x^\alpha u + (\nabla_y^\alpha)^* \nabla_y^\alpha u \right) \eta \, dy \\ &\quad + \gamma \int_{\Omega} \frac{(\nabla_x^\alpha)^* \nabla_x^\alpha u + (\nabla_y^\alpha)^* \nabla_y^\alpha u}{|\nabla^\alpha u|} \eta \, dy \\ &\quad + \lambda \int_{\Omega} (u - u_0) \eta \, dy \end{aligned} \quad (22)$$

For $\eta \in C^\infty(\Omega)$, we have

$$\begin{aligned} \varphi c(|\nabla^\alpha u|^2, PA^2) \left((\nabla_x^\alpha)^* \nabla_x^\alpha u + (\nabla_y^\alpha)^* \nabla_y^\alpha u \right) \\ + \gamma \frac{(\nabla_x^\alpha)^* \nabla_x^\alpha u + (\nabla_y^\alpha)^* \nabla_y^\alpha u}{|\nabla^\alpha u|} + \lambda(u - u_0) = 0 \end{aligned} \quad (23)$$

Let $E(u) = \int_{\Omega} \left(\varphi c(|\nabla^\alpha u|^2, PA^2) \left((\nabla_x^\alpha)^* \nabla_x^\alpha u + (\nabla_y^\alpha)^* \nabla_y^\alpha u \right) + \gamma \frac{(\nabla_x^\alpha)^* \nabla_x^\alpha u + (\nabla_y^\alpha)^* \nabla_y^\alpha u}{|\nabla^\alpha u|} + \lambda(u - u_0) \right) \eta \, dy$. Then $\nabla E = 0$. Thus, $\nabla E = 0$.

$$\begin{aligned} \nabla E = \varphi c(|\nabla^\alpha u|^2, PA^2) \left((\nabla_x^\alpha)^* \nabla_x^\alpha u + (\nabla_y^\alpha)^* \nabla_y^\alpha u \right) \\ + \gamma \frac{(\nabla_x^\alpha)^* \nabla_x^\alpha u + (\nabla_y^\alpha)^* \nabla_y^\alpha u}{|\nabla^\alpha u|} + \lambda(u - u_0) \end{aligned} \quad (24)$$

Thus, we have $\nabla E = 0$. By [63], we have $\Delta t u^{n+1} = u^n + \Delta t(-\nabla E)$. From (24), we have $\nabla E = 0$.

C. Numerical Algorithm

Let $\Omega = [0, X] \times [0, Y]$. We discretize Ω by $X \times Y$ grid. Let $u = u_{i,j}$ be the value of u at the grid point (i, j) . Then, we have

$$\begin{cases} \nabla_x^\alpha u_{i,j} = \sum_{l=0}^j (-1)^l \binom{\alpha}{l} u_{i,j-l} \\ \nabla_y^\alpha u_{i,j} = \sum_{l=0}^i (-1)^l \binom{\alpha}{l} u_{i-l,j} \end{cases} \quad (25)$$

$$\begin{cases} (\nabla_x^\alpha)^* u_{i,j} = \sum_{l=0}^{Y-1-j} (-1)^l \binom{\alpha}{l} u_{i,j+l} \\ (\nabla_y^\alpha)^* u_{i,j} = \sum_{l=0}^{X-1-i} (-1)^l \binom{\alpha}{l} u_{i+l,j} \end{cases} \quad (26)$$

Algorithm 1 PFDTV FRACTIONAL ANISOTROPIC DIFFUSION AND TOTAL VARIATION

Input:

TABLE II
COMPARISON OF THE PSNR, MSSIM AND FSIM VALUES AMONG DIFFERENT FILTERS



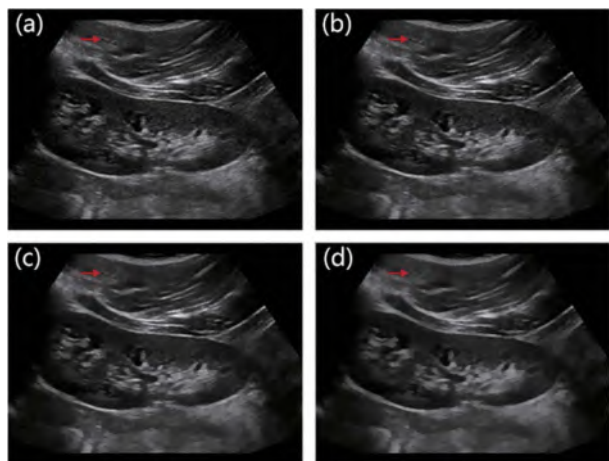


Fig. 4. Experimental results of denoising with different k_0 values. (a) Original image. (b) $k_0 = 5$. (c) $k_0 = 20$. (d) $k_0 = 100$.

Table 1. Comparison of denoising performance between the proposed method and other methods. The table lists the Mean Structural Similarity Index (MSSIM) and Peak Signal-to-Noise Ratio (PSNR) for three different denoising methods: MSSIM, PSNR, and PFDTV. The proposed method shows superior performance in both metrics across all three methods.

B. Clinical Image Experiment

In this section, we present the experimental results of the proposed method on clinical ultrasound images. The images are denoised using the proposed method with different parameters. The results are compared with other methods. The proposed method shows superior performance in both metrics across all three methods.

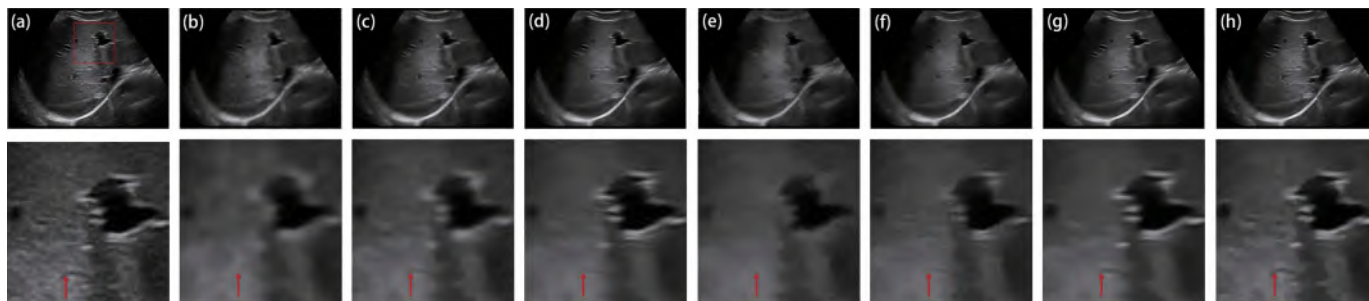


Fig. 6. Denoising results of the original image using SRAD, OBNLM, SBF, ADLG, NLLRF, and PFDTV. (a) Original image, (b) SRAD, (c) OBNLM, (d) SBF, (e) ADLG, (f) NLLRF, and (g) PFDTV.

Fig. 7. Denoising results of the original image using SRAD, OBNLM, SBF, ADLG, NLLRF, and PFDTV. (a) Original image, (b) SRAD, (c) OBNLM, (d) SBF, (e) ADLG, (f) NLLRF, and (g) PFDTV.

SRAD, OBNLM, SBF, ADLG, NLLRF, and PFDTV. In Fig. 7, SRAD, OBNLM, NLLRF, and SBF are unable to remove the speckle noise. OBNLM and NLLRF are unable to remove the speckle noise. SRAD, ADLG, and PFDTV are able to remove the speckle noise. ADLG and PFDTV are able to remove the speckle noise.

Fig. 8. Despeckling results of the ROI in Fig. 7(a) using different methods: (a) OBNLM, (b) SBF, (c) ADLG, (d) NLLRF, and (e) PFDTV.

... DSC JS ...
 ... A ...
 ... HD HM ...
 ... H n ...
 ... DSC JS, ... HD ...
 HM. T_{III} T_{IV} ...
 DSC, JS, HD HM ...
 ... BUS ... O ... PFDTV ...
 ... DSC JS ...
 HD HM ... PFDTV ...
 ...
 T ... OBNLM, NLLRF ...
 PFDTV ...
 In (R) C r (TM) CPU 2.71 GH 8 GB
 RAM. T ... Fr. 7(a)
 225×300 ... 86.54 ... OBNLM ...
 2.85 ... NLLRF ...
 430.21 ... A ... PFDTV ...

		HD	HM
IP	38.02	16.9933	3.3599
Fros	38.02	9.8418	2.1265
SRAD	38.02	8.2271	1.5781
OBNLM	38.02	8.2271	1.5781

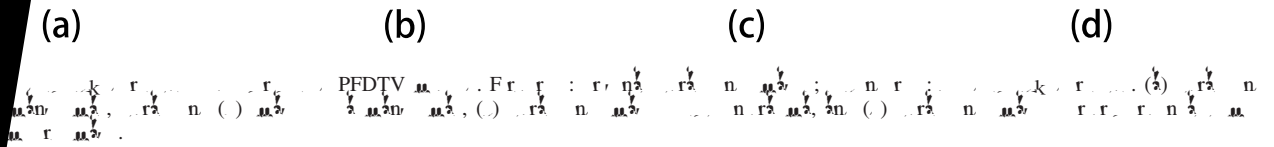


Fig. 10. Ten breast ultrasound images. (a) Ground truth, (b) T, (c) SRAD, (d) OBNLM, (e) SBF, (f) ADLG, (g) NLLRF, (h) D, (i) Y, (j) PFDTV.

TABLE IV
THE MEDIAN DSC, JS, HD AND HM VALUES FOR DIFFERENT SEGMENTATION RESULTS ON TEN BREAST ULTRASOUND IMAGES

- [29] A. S. L., H. M., P., A. n. *Measurement*, . . . 140, . . . 572-581, J. . . 2019.
- [30] D. G., R. S. An., B. T., S. k. *IET Image Process.*, . . . 9, n. 2, . . . 107-117, 2015.
- [31] Z. Q., L. Y., W. L., A. n. *Proc. BMVC*, 2011, . . . 73.
- [32] V. B. S. Pr., R. P., G. S., K. P., M. *IEEE Trans. Image Process.*, . . . 28, n. 12, . . . 6198-6210, Dec. 2019.
- [33] N. O., M. G., S. A., A. Br., B. N., R. B., On *IEEE Trans. Pattern Anal. Mach. Intell.*, . . . : 10.1109/TPAMI.2019.2892134.
- [34] R. C., R., R. S., L. M., H. B., A. n. *arXiv:1904.10235*. [Online]. Available: //arxiv.org/abs/1904.10235
- [35] V. K., A. F., K. E., J. A., Fr. *Int. J. Comput. Vis.*, . . . 86, n. 1, . . . 1-32, 2010.
- [36] H. T., S. F., P. M., K. m., n. r. *IEEE Trans. Image Process.*, . . . 16, n. 2, . . . 349-366, Feb. 2007.
- [37] B. Q., Z. S., Z. Z., J. Z., Y. L., S. r. *Appl. Soft Comput.*, . . . 46, . . . 851-867, Sep. 2016.
- [38] B. Q., Z. S., Z. F., Z. Z., Y. L., J. B., J. n. *IEEE Access*, . . . 6, n. 1, . . . 330-343, 2018.
- [39] L. Z., W. W., J. Q., K.-H. W., K.-S. C., P.-A. H., F. *Signal Process.*, . . . 134, . . . 275-284, Mar. 2017.
- [40] A. B., D. B., Y. M., P. *IEEE Trans. Inf. Technol. Biomed.*, . . . 15, n. 1, . . . 138-147, Jan. 2011.
- [41] M. C. M., J. R., D. C. B., R. O., M. *Nature*, . . . 324, n. 6049, . . . 250-253, Nov. 1986.
- [42] M. C. M., R. A. O., F. *Pattern Recognit. Lett.*, . . . 6, n. 5, . . . 303-313, Dec. 1987.
- [43] M. M., P., J. A. N., 2D+T. *Med. Image Anal.*, . . . 4, n. 1, . . . 21-30, 2000.
- [44] P. K., I. *J. Comput. Vis. Res.*, . . . 1, n. 3, . . . 1-26, 1999.
- [45] G.-Q. Z., W.-W. J., K.-L. L., Y.-P. Z., A. *IEEE Trans. Med. Imag.*, . . . 36, n. 6, . . . 1250-1262, Jun. 2017.
- [46] Q. Z., J. G., Z. W., K. L., A. *IEEE Trans. Geosci. Remote Sens.*, . . . 54, n. 4, . . . 1905-1917, Apr. 2016.
- [47] J. Y., L. T., S. Z., L. W., M. A. S., I. *IEEE Access*, . . . 5, . . . 12275-12285, 2017.
- [48] V. M., P. R., M. S. P., M. *IEEE Trans. Image Process.*, . . . 19, n. 5, . . . 1138-1152, May 2010.
- [49] J. P. H., P. T., A. C. B., AM-FM. *Handbook of Image and Video Processing*. A. n. T. N. : E. 2005, . . . 377-395.
- [50] M. C., T. O., V. P., T.

[76] B. Guo, A. Durr, S. Avramovic, B. S. Sankaranarayanan, and A. Sankaranarayanan, "Fractional anisotropic diffusion for despeckling of medical ultrasound images," *Inf. Fusion*, vol. 55, pp. 220–244, Mar. 2020.

[77] C. A. N. Sankaranarayanan, N. D. A. Mankaranarayanan, and G. Bhanu, "Fractional anisotropic diffusion for despeckling of medical ultrasound images," *IEEE Trans. Image Process.*, vol. 28, no. 1, pp. 216–226, Jan. 2019.

[78] Y. Jiang, X. Jiang, and W. Jiang, "Anisotropic fractional diffusion for despeckling of medical ultrasound images," *J. Vis. Commun. Image Represent.*, vol. 65, Dec. 2019, Art. no. 102661, doi:10.1016/j.jvcir.2019.102661.

[79] Y. F. Peng et al., "Anisotropic fractional diffusion for despeckling of medical ultrasound images," *IEEE Trans. Image Process.*, vol. 27, no. 3, pp. 1214–1229, Mar. 2018.

[80] F. Zhang et al., "Robust fractional anisotropic diffusion for X-ray image denoising," *Phys. Med. Biol.*, vol. 58, no. 6, pp. 1739, 2013.

[81] R. J. G. Simons, R. C. Chen, and Y. C. Eldner, "Deep learning for medical ultrasound despeckling," *Proc. IEEE JPRQC.2019.2932116*.

[82] X. Jiang, S. Li, X. Feng, and L. Zhang, "FOCN: A fractional order non-local convolutional network for medical ultrasound image denoising," *Proc. IEEE Conf. Comput. Vis. Pattern Recognit.*, Jun. 2019, pp. 6054–6063.



Bin Hu received M.S. and Ph.D. from Tsinghua University in 1997 and 2000, respectively. He received his M.D.-P.D. from Shandong University in 2006. He is currently an associate professor and the director of the Shandong Provincial Key Laboratory of Medical Ultrasound, Shandong University. He has published over 30 papers in international journals and conferences. His research interests include medical image processing, computer vision, and machine learning.



Baowei Fei received M.S. and Ph.D. degrees from Case Western Reserve University, Cleveland, OH, USA, in 1999 and 2002, respectively. He is currently an associate professor and the director of the Center for Ultrasound Image Processing and Analysis, Texas A&M University, Houston, TX, USA. He has published over 50 papers in international journals and conferences. His research interests include medical image processing, computer vision, and machine learning.



Kunqiang Mei received B.S. and M.S. degrees from Nanjing University of Aeronautics and Astronautics, Nanjing, China, in 2016 and 2019, respectively. He is currently a Ph.D. student at Tsinghua University, Beijing, China. His research interests include medical image processing, computer vision, and machine learning.



Binjie Qin (M'07) received M.S. and Ph.D. degrees from Nanjing University of Aeronautics and Astronautics, Nanjing, China, in 1999 and 2002, respectively. He is currently an associate professor and the director of the Shandong Provincial Key Laboratory of Medical Ultrasound, Shandong University. He has published over 30 papers in international journals and conferences. His research interests include medical image processing, computer vision, and machine learning.